UC San Diego

UC San Diego Previously Published Works

Title

MRI-based mechanical competence assessment of bone using micro finite element analysis (micro-FEA): Review.

Permalink

https://escholarship.org/uc/item/0sc3q7bf

Authors

Jerban, Saeed

Alenezi, Salem

Afsahi, Amir

et al.

Publication Date

2022-05-01

DOI

10.1016/j.mri.2022.01.009

Peer reviewed

eScholarship.org Powered by the California Digital Library
University of California

Author Manuscript

Author Manuscript

Author Manuscript

Author Manuscript

HHS Public Access

Author manuscript

Magn Reson Imaging. Author manuscript; available in PMC 2022 May 01.

Published in final edited form as:

Magn Reson Imaging. 2022 May ; 88: 9–19. doi:10.1016/j.mri.2022.01.009.

MRI-based mechanical competence assessment of bone using micro finite element analysis (micro-FEA): review

Saeed Jerban[1,*], **Salem Alenezi**[2], **Amir Masoud Afsahi**[1], **Yajun Ma**[1], **Jiang Du**[1], **Christine B. Chung**[1], **Eric Chang**[3,1,*]

[1]Department of Radiology, University of California, San Diego, CA, USA

[2]Research and Laboratories Sector, Saudi Food and Drug Authority, Saudi Arabia

[3]Research Service, Veterans Affairs San Diego Healthcare System, San Diego, CA, USA

Abstract

Areal bone mineral density (aBMD) from dual-energy x-ray absorptiometry (DEXA) and volumetric bone mineral density (vBMD) have demonstrated limited capabilities in the evaluation of bone mechanical competence and prediction of bone fracture. Predicting the macroscopic mechanical behavior of the bone structure has been challenging because of the heterogeneous and anisotropic nature of bone, such as the dependencies on loading direction, anatomical location, and sample dimensions. Magnetic resonance imaging (MRI) has been introduced as a promising modality that can be coupled with finite element analysis (FEA) for the assessment of bone mechanical competence. This review article describes studies investigating MRI-based micro-FEA as a potential non-invasive method to predict bone mechanical competence and facilitate bone fracture risk estimation without exposure to ionizing radiation. Specifically, the steps, applications, and future potential of FEA using indirect and direct bone imaging are discussed.

Keywords

MRI; micro finite element analysis; cortical bone; trabecular bone; mechanical competence

1. Background

Areal bone mineral density (aBMD), as measured by dual-energy x-ray absorptiometry (DEXA) at the spine or hip, is the standard clinical determinant in bone fracture risk assessment [1–3]. Despite the widespread use of aBMD in clinics, a diagnosis of osteoporosis (based on DEXA T-score <−2.5) often fails to predict fracture risk accurately [4–6], with reported prediction rates between 30% and 50% when used alone [7–15]. For instance, the observed decrease in aBMD from age 60 to 80 accounts for a doubling of

[*]**Corresponding authors: Eric Y. Chang,** Research Service, VA San Diego Healthcare System, 3350 La Jolla Village Drive, San Diego, CA 92161, USA, ericchang.2@va.gov, Phone: +1 858 246 2248, Fax: +1 888 960 5922; **Saeed Jerban,** Department of Radiology, University of California San Diego, 9500 Gilman Drive, San Diego, CA 92093, USA, sjerban@ucsd.edu, Phone : +1 858 246 3158, Fax : +1 888 960 5922.

6.Conflict of interest statement

The authors have no conflicts of interest to declare.

Author Manuscript Author Manuscript Author Manuscript Author Manuscript

the fracture risk, but it's known that overall fracture risk increases thirteen-fold during this period [5,10]. Specifically, DEXA-based aBMD is unable to detect local changes in bone structure due to the method's two-dimensional (2D) nature. The Fracture Risk Assessment (FRAX) tool, a computer-based algorithm, has been recently proposed as an alternative and/or complementary measure to aBMD. FRAX predicts the ten-year probability of hip fracture or a major osteoporotic fracture in patients based on a set of clinical and social risk factors, including aBMD, age, sex, fracture history, body mass index (BMI), and smoking history [16]. However, just as is the case with aBMD, FRAX fails to consider the local changes in bone structure for fracture risk assessment, hampering its accuracy and usefulness. As a consequence, it's clear that alternative techniques that are capable of assessing bone mechanical competence under specific loading conditions are necessary to fill this gap.

Predicting mechanical properties of bone, particularly in trabecular bone sites, is challenging because of the heterogeneous and anisotropic nature of bone, such as the dependencies on loading direction, anatomical location, and sample dimension [17,18]. Ulrich et al. [19] have specifically shown the difference between elastic moduli in trabecular bone can be up to 53% for bone specimens with a certain volume fractions or vBMD. Finite element analysis (FEA) coupled with high-resolution three-dimensional (3D) medical imaging techniques (i.e., micro-FEA) has been increasingly used for assessment of bone mechanical competence. In micro-FEA, the displacements, forces, as well as stress and strain tensors can be calculated throughout the meshed volume of the specimen including all trabeculae for different boundary conditions.

Although, Although, homogenized FE models using low resolution images (large elements including trabeculae and marrow) can be used for trabecular bone assessment [17,20], micro-FEA has been hypothesized to improve the prediction of the experimental mechanical properties over homogenized FE [17,21]. This is due to high anisotropy and heterogeneity levels in the trabecular bone, particularly at certain sites such as the hip [17,20,22]. In cases where the achievable voxel sizes are much higher (e.g., >0.5 mm) than the trabeculae thickness (100 to 200 micrometers [23]) or where a semi-uniform principal trabecular orientation can be assumed (e.g., cranio-caudal direction in vertebrae) [20], homogenized FE models would be the best option. In addition to homogenized and micro-FE models, multiscale FE models have also been proposed which include several intermediate levels, in which bone material characteristics are updated based on the changes of porosity and geometry in different material scales [24,25]. It should be noted that the current review study is only focused on micro-FEA. Computer memory demands were previously a major barrier to the feasibility of micro-FEA for widespread clinical application, but recent advances in FEA software and desktop computer performance have led to the steady rise of micro-FEA applications in research and clinical settings [26–31]. It should be noted that the micro-FEA accuracy generally increases by increasing the number of elements in the micro-FE models, which requires higher image resolution, larger datasets, and longer computation times for FE algorithms [17,24,25].

Microcomputed tomography (μCT) has been the primary preferred technique for performing ex vivo micro-FEA in order to assess the mechanical competence of trabecular bone

Author Manuscript Author Manuscript Author Manuscript Author Manuscript

[22,32,33]. Other high-resolution x-ray-based imaging techniques, such as high-resolution peripheral quantitative computed tomography (HR-pQCT), have also been used in FEA studies to predict the mechanical competence of bone structure [34–36]. For example Orwoll et al. [37] studied the correlations between FEA results and the risk of hip fracture in older men and reported that the femoral strength and the load-to-strength ratio obtained from QCT-based FEA were strongly associated with the hip fracture risk. Keyak et al [38] studied the effect of loading condition on the association between incident hip fracture and hip strength obtained from QCT-based FEA. They reported that specifically posterolateral loading in men and posterior loading in women were most strongly associated with incident hip fracture [38]. Despite the benefits of performing QCT-based FEA, researchers need to make sure that the benefits of the required CT scans for each individual outweigh the potential harm caused by ionizing radiation (e.g., 1–3 millisieverts (mSv) effective dosage for a total hip QCT scan despite ~0.001 mSv in DEXA) [20,39]. It should be noted that such a radiation exposure is not significantly more than the average annual background radiation (~1 mSv), although dose would be much higher if QCT were to be used at other sites of interest, such as the lumbar spine.

In the past two decades, high-resolution magnetic resonance imaging (MRI) has been demonstrated as a promising modality for in vivo bone imaging in cortical and trabecular sites and which can be coupled with FEA for the assessment of bone mechanical competence [40–44]. Unlike HR-pQCT, MRI is capable of imaging both the appendicular [45,46] and axial [47,48] skeleton. Furthermore, MRI is able to obtain complementary information from surrounding soft tissues such as bone marrow [49,50], tendon [51], cartilage [52], and muscle during the same scan session. This complementary information may provide an opportunity to assign more accurate boundary conditions in FE models, although this remains to be further studied. Although, utilizing such complementary information has not been reported in the literature to the authors' knowledge, but they can be employed to assign more accurate boundary conditions in FE models.

This review article describes studies of MRI-based micro-FEA as a potential means to predict bone mechanical competence and facilitate non-invasive bone fracture risk estimation. Various MRI techniques that have been used to render bone microstructure are described. Reviewed MRI-based FEA studies are summarized in Table 1. Future potential pathways to more accurate MRI-based micro-FE models are also discussed.

2. FEA studies based on indirect bone imaging

Indirect bone imaging has been used as the input for finite element (FE) models in several investigations. This chapter describes the steps of MRI-based micro-FEA using indirect bone imaging and is concluded by a summary of reported applications in the literature.

2.1 Steps of MRI-based FEA

Standard clinical MR imaging can indirectly visualize both trabecular and cortical bone as dark regions surrounded by bright signal from bone marrow and other soft tissues. Bone possesses low water content and a short T2 relaxation time, resulting in voided signal when

Author Manuscript Author Manuscript Author Manuscript Author Manuscript

imaged with conventional MRI sequences. 3D bone microstructure can be extracted by post-processing of the MRI images for use as input in FE models [45,47,48,53,54].

Both high-resolution spin-echo (SE) and gradient-recalled echo (GRE) MRI sequences have been used for high-resolution trabecular bone imaging [46]. SE-based sequences produce lower signal intensity distortion in trabecular bone structure and more accurate trabeculae dimensions [46], while GRE-based techniques result in shorter scan times because of a shorter achievable repetition time (TR) [46]. Considering the average thickness of human trabecular bone, ranging from 100 to 200 micrometer [23], the in-plane MRI pixel sizes are often selected to be below 0.2 mm, enabling the detection of trabeculae in healthy human subjects. MR images at such resolutions are referred to as “high-resolution MR images” in the context of this review article. Two examples of visualized trabecular bone as dark pixels surrounded by bright bone marrow are shown in Figure 1 (A: fast large-angle spin-echo (FLASE), B: GRE-based sequence, balanced steady-state free precession (bSSFP)) [46]. Fast SE techniques have been also used to visualize the cortical bone microstructure including the haversian canals [55].

FE model preparation process can start with application of a filter algorithm for image inhomogeneity compensation across the volume of interest due to variation in spatial sensitivity of the MR receive coil [56]. However, inhomogeneity compensation may be skipped depending on coil sensitivity variation levels and the positioning of the bone interest in the scanner. The resulting images are then processed (e.g., inverting the contrast, smoothing, etc.) and segmented in order to generate a 3D matrix of bone volume fraction (BVF). It should be noted that the conventional MRI signal from bone has been assumed to include pore water and fat signals (residing in inter and intra-trabecular spaces) which correlates with the bone porosity. Therefore, inverted MRI signal would correlate with the solid bone volume in each voxel. The value assigned to each voxel in the BVF matrix is assumed to be equal to the fractional occupancy of bone, calculated as bone volume divided by total volume (BV/TV) in that specific voxel [57]. The difference in the obtained gray level for different voxels in an MR image has been assumed to be the result of partial voluming. It should be noted that a partial threshold has been empirically determined and contributions from image noise can be removed by setting elements with BVF<20% to zero [58]. However, such thresholds should be revisited when other MRI scanners or sequences are used. Using low or high thresholds may result in bone overestimation or underestimation, respectively, which is a general challenge in both MRI and CT-based FEA studies [44,59]. Bone overestimation errors as a result of low BVF thresholds can be reduced by considering the element’s material property as a linear function of its BVF value, as described below. Specifically, although some voxels with low BVF may be erroneously included in the model, the low assignment of material properties to those voxels will prevent them from having a large impact on the FEA result.

In order to generate the FE model, bone voxels in the BVF map can then be directly converted to hexahedral elements (brick) with dimensions equal to the voxel size. The element generation process is called FE meshing. In most studies, the tissue material properties for each element have been assumed to be isotropic and linearly elastic. Assuming isotropic material properties for bone elements can be challenging [18,60]. For example,

Author Manuscript Author Manuscript Author Manuscript Author Manuscript

cortical bone has demonstrated significantly different stiffness in the longitudinal direction compared with the radial direction[18].

Material behavior in FE models can be considered as linear elastic or non-linear elastic-perfectly-plastic. Basically, the bone elasticity is its ability to resist deformation under mechanical load and to return to its original shape once the load is removed. Bone elastic behavior is assumed to be linear (linear relationship between stress and strain) while the applied stress remains below the bone yield point (e.g., corresponding to strains <1%[20]), as exists during normal daily activities [17]. Linear elastic FE models enable linear mechanical properties to be calculated such as the apparent stiffness of the modeled structure (Young's modulus, E, for normal loading and shear modulus, G, for tangential loading)[20]. Bone plasticity is the ability to endure a non-reversible permanent deformation under the applied load, which happens after the yield point until the ultimate failure of the structure [20,61]. In linear elastic FE models, the elastic modulus (E) of each element can be set to a constant value (when the BVF matrix is considered as a binary matrix, BVF = 0% or 100%)[40–44,62]) or a linear function of its corresponding BVF value such that $E = E0 \times BVF$ (where E0 is bulk bone elastic modulus) [30,63]. Using linear elastic models generally enables us to calculate bone stiffness (i.e., effective elastic modulus for the modeled structure) which has been reported in several MRI-based micro-FEA studies. FEA studies require the use of a material failure criterion for bone strength estimation and for prediction of the anatomical locations of where failure is initiated. In linear elastic FE models, failure criteria are generally computed based on the strain distribution over the modeled structure [17,20]. A typical failure definition in linear elastic FE models is when the fraction of bone volume or elements (e.g., 2%) exceeds a given strain level (e.g., 0.7% strain) [64,65]. It should be noted that any hypothesized failure criteria require a thorough validation process using experimental tests for any FE model including its imaging, meshing, and material failure criteria. To the authors' knowledge the reported linear micro-FEA studies have only investigated stiffness, not strength.

Nonlinear elastic-plastic FE models have been proposed to take into account the plastic deformation of bone as the applied stress increases (e.g., corresponding to strains >3%) [20,26]. Material failure criterion in such models can be described by adding the post-yield material behavior to the linear elastic behavior. Investigating the post-yield material stress allows for estimation of the ultimate strength and predicton of the anatomical locations where failure is initiated. In such a nonlinear model, the post-yield bone stress-strain relationship can be simplified using different methods. For example, in elastic-perfectly plastic behavior, the plastic flow of the material starts when stress reaches the yield point (strain increases indefinitely without increasing the stress)[66]. Since the materials in experimental tests have demonstrated a softening behavior before complete failure (i.e., the material still resists under mechanical stress but stiffness decreases)[18], some studies have considered multiple steps to model plastic flow. The first phase is assumed to be a perfectly-plastic flow that initiates at the yield point until the plastic strain reaches a certain value, the second phase (strain softening) occurs with a decreasing plastic modulus until a certain stress level is reached, and the third phase is a perfectly-plastic phase that follows indefinitely [66]. Zhang et al. [26] performed the first MRI-based micro-FEA investigation using non-linear elastic-plastic material modeling, using a power function of

Author Manuscript Author Manuscript Author Manuscript Author Manuscript

the hyperbolic tangent in an effort to simulate the softening plastic behavior of the material. The material nonlinearity could be simulated by iteratively adjusting the element's elastic modulus based on the element-level effective strain. Figure 2 shows strain maps generated for two representative distal tibial bone specimens: one with high mechanical properties (Figure 2A) and the other with low mechanical properties (Figure 2B).

2.2. FEA studies based on indirect bone imaging

In most of the initial MRI-based micro-FEA studies, investigated bone sites were limited to locations that permitted the use of either closely fitted volume transmit-receive coils or surface coil arrays to provide adequate signal-to-noise ratio (SNR) in high resolution images. All micro-FEA discussed studies in this section are based on indirect imaging of bone where bone itself is visualized as a dark region surrounded by bright bone marrow and other soft tissues.

Van Rietbergen et al. [40] were pioneers in estimating the mechanical properties of trabecular bone by using linear FE models on MR images at 1.5T. They used a modified fast GRE sequence to image trabecular bone in human femoral head bone specimens at 117×117×300 μm^3 voxel size. A constant elastic modulus was set to each generated element (i.e., E = 10 GPa) and an in-house developed FE solver was used for FEA. They found that the results of the MR-based FE models compared well qualitatively with μCT-based FE models, though some correction factors were required to achieve accurate values. Later, a similar MRI-based FEA study was performed by Newitt et al. [41] in vivo on distal radius at 1.5T using a fast GRE sequence at 156×156×500 μm^3 voxel size. They compared FEA results between post-menopausal women with normal aBMD and those with low aBMD (i.e., osteoporosis or osteopenia). Normal and shear elastic measures were found to be lower in the low aBMD group compared with the normal group. In another study, the same group used MRI-based micro-FEA to study changes in the mechanical properties of bone in post-menopausal women after one year of idoxifene treatment. A fast GRE sequence was used at 1.5T to image the calcaneal trabecular bone at 195×195×500 μm^3 voxel size [43]. Significant changes were observed in estimated mechanical properties from baseline within groups after one year of treatment. Newitt et al. [42] later investigated the reproducibility of their FEA method by using MR images performed on the distal radius including trabecular bone alone. They reported that the estimated Young's and shear moduli varied by 4-9% with coefficients of variation in the range of 20-38%. A few years later, Alberich-Bayarri et al. [62] used a 3D spoiled T1-weighted GRE sequence at 180 μm isotropic voxel size on a 3T scanner to develop FE models and investigated the gender-based differences in mechanical properties of trabecular bone at the distal radius. FE-based elastic modulus was found to be significantly different between men and women subjects. Rajapakse et al. [44] compared FE models derived from MR images on a 9.4T scanner at 50 μm isotropic voxel size with models from μCT at 21 μm. This study was a validation study performed on cadaveric specimens. The 3D SE sequence was used to image the trabecular bone specimens from proximal tibia, proximal femur, and lumber vertebrae. Similar to the previously mentioned investigations, they used a constant elastic modulus for all bone elements (E = 15 GPa). Significant strong correlations were observed between estimated moduli from μCT and MR-based FEA [44].

Author Manuscript Author Manuscript Author Manuscript Author Manuscript

It should be noted that in all reviewed linear MRI-FEA studies, the mechanical competence outcome has been stiffness. The simulated loading has been limited to the elastic region of the stress-strain curve (for example ~1% strain boundary conditions in the compression tests [58]) to avoid potentially including the yield point of the structure. High correlations between the yield strength and stiffness have been assumed in such linear FEA studies because pure elastic materials have been assigned to the elements. Notedly, bone stiffness has shown high correlation with ultimate strength in experimental tests, though the correlation coefficients depend on the age and sex of the donors [67].

Later, by improving FE solvers, more sophisticated MRI-based micro-FE models were investigated using non-constant elastic modulus for bone elements. Rajapakse et al. [28] compared the estimated mechanical parameters from such MRI-based FEA performed on a clinical scanner (1.5T) at 160 μm isotropic voxel size with parameters derived from μCT-based models at 25 μm isotropic voxel size. MRI 3D FLASE pulse sequence was used to image the trabecular bone samples. Despite previous MRI-based FEA models, the elastic modulus of each bone element was set to be a linear function of BVF. Before BVF calculation, the image intensity was corrected to compensate for coil inhomogeneity. They reported that the elastic and shear moduli of cadaveric tibia at trabecular bone sites derived from MRI were significantly correlated with those derived from volume-matched reference μCT images. Liu et al. [68] later used the same method to compare the MRI and μCT-based FEA performed on proximal tibial trabecular bone covering whole-bone (not only trabecular bone). In addition to significant correlations between microstructural parameters, they reported strong correlations between estimated mechanical properties from MRI and μCT-based FEA. The whole-bone and trabecular bone stiffness based on MRI were highly correlated with μCT-based results, suggesting that MRI-based FEA can directly and accurately quantify whole-bone mechanical competence. Nevertheless, rigorous validation requires comparing FEA results with experimental mechanical tests. Wehrli et al. [69] used a similar method [28,68] to investigate the impact of estrogen supplementation on bone mechanical competence in early post-menopausal women. FE models were generated from MRI images of trabecular bone in the distal radius and distal tibia in vivo. FEA revealed significant reduction in mechanical competence in the control group over time, but a significant increase in mechanical competence was observed in treated groups over one and two-year follow-up visits [28,68]. Rajapakse et al. [63] later utilized their own developed MRI-based micro-FEA analysis to study the changes in mechanical competence of cortical and trabecular bone after renal transplantation. This in vivo longitudinal study was focused on trabecular bone and cortical bone in the distal tibia and performed using FLASE sequence on a 1.5T scanner at 137×137×410 μm voxel size. They found that FEA-based mechanical competence was significantly lower at 6 months after renal transplantation compared with baseline for cortical, trabecular, and whole-bone models. Interestingly, significant reductions in mechanical competence were concurrent with only nonsignificant bone microstructural changes.

To improve the translatability of the MRI-based bone FEA to in vivo studies, MRI sequences appropriate for faster trabecular bone imaging, such as 3D fast low angle shot (FLASH) sequence, have been recently developed. Chang et al. [70] performed an in vivo estimation of bone stiffness through FEA at the distal femur and proximal tibia on a 7T scanner using

Author Manuscript Author Manuscript Author Manuscript Author Manuscript

3D FLASH sequence. The FE models were generated for whole, cortical, and trabecular bone on MRI images at 234×234×1000 μm voxel size. Similar to previously described studies, FEA was performed for compression loading. They showed that at the distal femur and proximal tibia (near knee joint), trabecular bone contributed approximately twice the contribution of cortical bone in whole bone stiffness. Chang et al. [71] later used similar FLASH MRI images and linear MRI-based FE models to study improvements in bone mechanical competence of the distal femur in female pre-professional dancers. They found greater whole and cancellous bone stiffness, but not greater cortical bone stiffness, in the distal femur of female dancers compared to control subjects. This might be due to the lack of information in cortical bone quality accessible by indirect bone imaging.

Later, by developing more appropriate MRI sequences for high resolution trabecular bone imaging, additional bone sites became accessible for MRI-based FEA. Chang et al. [72] used linear FEA based model on MRI images of the proximal femur at 3T and showed lower bone stiffness (elastic modulus) in patients with fragility fractures compared with control subjects. This was the first MRI-based FEA study performed in vivo on the proximal femur, made possible mainly because of SNR gains from multichannel coils and SNR efficient pulse sequences [47,48]. While a significant difference in mechanical competence was found, no difference in aBMD was observed. The FLASH sequence was used to image the proximal femur at 234×234×1500 μm. Later, Chang et al. [73] investigated the reproducibility of such MRI-based FEA at the proximal femur for sideway-fall loading on trabecular bone. The same MRI acquisition sequence and parameters were used to scan subjects three times on separate days. The measured reproducibility level showed that the FEA-based assessment of proximal femur stiffness using MRI was suitable for clinical studies of disease progression or treatment response [73].

The feasibility of using nonlinear FEA based on in vivo MRI images was investigated for the first time by Zhang et al. [26] in order to estimate post-yield properties of trabecular bone. The nonlinear model enabled simulations of trabecular bone yield and post-yield behavior from MRI at in vivo resolution by solving a series of nonlinear systems (i.e., $E = \left(\left(\mathrm{sech}(50 \times \varepsilon + 0.53)^{1.4}\right)^{0.6} + 0.05\right) \times BVF \times 15GPa\right)$ [26]. This longitudinal MRI-based FEA study was performed on patients from an ongoing interventional study who were taking drugs to manage osteoporosis. Zhang et al. [27] later used the same MRI-based FEA method to assess mechanical competence (yield strain/strength, ultimate strain/strength, modulus of resilience, and toughness) at the distal radius of pre-menopausal and post-menopausal women and reported adequate reproducibility level to evaluate treatment effects in interventional studies. Recently, Rajapakse et al. [31] investigated the reproducibility level of non-linear MRI-based FEA performed on the proximal femur. Similar studies were performed before for linear MRI-based FEA [73]. FLASH sequence was used to acquire images at 234×234×1500μm voxel size. For all estimated mechanical parameters (stiffness, yield strain, yield load, ultimate strain, ultimate load, resilience, and toughness) in stance and sideways-fall loading, the coefficient of variations (standard deviation divided by the average value) was below 10%, while the intraclass correlation coefficient was above 0.99. The reproducibility study comprised of A) test-retest reproducibility analysis where13 subjects underwent MR imaging on 3 separate occasions), B) inter-operator

Author Manuscript Author Manuscript Author Manuscript Author Manuscript

reproducibility analysis where a single MRI was performed on 10 subjects and four operators independently performed the analysis, and C) intra operator reproducibility analysis, where the analysis was performed two times by each analyst for those single MRI on 10 subjects. This experiment demonstrated that the FEA can consistently and reliably provide fracture risk information. More recently, Rajapakse et al. [30] validated MRI-based FEA performed on distal tibial specimens using mechanical compression tests. The FLASE sequence was performed on a 3T scanner to acquire images at 137×137×410 μm voxel size. Linear and non-linear FE models were generated and then the stiffness, yield strength, ultimate strength, modulus of resilience, and toughness, were compared to experimental mechanical properties. Moderate to strong positive correlations were found between computationally and experimentally derived values of stiffness, yield strength, ultimate strength, and resilience [30]. Remarkably, the correlation of experimental ultimate strength with computational stiffness (from linear FE model) was higher than its correlations with computational ultimate strength, toughness, resilience and other parameters from non-linear FE model [30]. Therefore, performing only linear FE models is likely adequate for predicting the fracture risk which is assumed to be related to experimental ultimate strength.

3. FEA studies based on direct bone imaging

In the abovementioned MRI-based micro-FEA studies, bone structure was visualized through indirect bone imaging (dark bone voxels surrounded by bright soft tissue voxels). Such dark bone voxels, except for those on the boundary with the partial volume, are generally considered to have similar material properties in the FE models. However, bone may contain different proportions of pores or organic matrix quality that subsequently result in different material properties. Using direct bone MR imaging, sub-voxel bone material differences (likely due to the microporosity level and the organic matrix quality) can be included in FEA. Specifically, major water and fat molecules in bone can reside in a range of pores with different sizes including Haversian canals (10-200 μm), lacunae (1-10 μm), and canaliculi (0.1-1 μm)[74,75]. Visualizing these micropores is not possible due to image resolution limitations in MRI or other available in vivo medical imaging techniques. However, estimating the volume of these pores and the corresponding microstructure is achievable using ultrashort echo time (UTE) MRI. Previous studies have shown significant correlations of bone UTE MRI properties with its microstructural properties using histomorphometry at 0.2 and μCT at 9 micron resolution [76–78] as well as with its mechanical properties [79–81]. Despite its potential benefits, FEA based on direct bone imaging has not been investigated. Direct bone imaging, particularly at trabecular bone sites, is technically challenging because of the fast signal decay of bone caused by its short T2 relaxation time [82].

Ho et al. [83] used the iterative decomposition of water and fat with echo asymmetry and least-squares estimation (IDEAL) MRI technique to separate fat signal from water signal in the patella and performed FEA to compare strain maps between females with and without patellofemoral pain. The bone microstructure used in their FE model was estimated using the water signal from bone. To the authors' knowledge, other MRI techniques for direct bone imaging have not been used for FEA studies.

Author Manuscript Author Manuscript Author Manuscript Author Manuscript

Direct cortical bone imaging has been performed using several UTE techniques that have resulted in accurate morphological and quantitative imaging of bone [80,84,85]. Basic UTE MRI sequences with nominal TEs around tens of microseconds can detect signals from bone [55,86]. Despite the high bone signal using UTE MRI imaging, it results in relatively low contrast. UTE MRI fractional indexes have been used for cortical bone imaging with improved contrast. Dual echo time UTE imaging was used to calculate the so-called porosity index (PI), which is the signal ratio between two MRI images, one with TE ≈ 0.05 ms and one with TE ≈ 2 ms [77]. The first echo image represents signal from both bound and pore water, and the second echo represents mostly pore water signal [77]. PI is hypothesized to be correlated indirectly with the solid bone fraction in each imaging voxel. Suppression ratio (SR) was another UTE MRI fractional index proposed for cortical bone imaging and its microstructural evaluation [87]. SR was defined as the ratio between bone UTE signal without long T2 suppression and bone UTE signal with long T2 suppression performed via Dual-IR-UTE or IR-UTE. SR is hypothesized to be directly correlated with the solid bone fraction in each imaging voxel. UTE with rescaled echo subtraction (UTE-RS) is among other fractional index methods that can visualize cortical bone [88]. In UTE-RS, the first echo image is scaled down so that signals from muscle and fat become lower than those from the second echo [88]. In the subtraction image, signals from muscle and fat are negative, whereas those from short-T2 species are positive, separating them from air which has a signal intensity fluctuating around zero [88]. In addition to the UTE fractional indexes, adiabatic inversion recovery (IR) preparation pulses have been suggested in different studies to overcome the low contrast in UTE MR imaging of cortical bone. Specifically, a relatively long adiabatic IR pulse is employed to simultaneously invert the longitudinal magnetizations of long T2 water and fat [89–93]. The UTE data acquisition starts at an inversion time (TI) designed to allow the inverted free water and fat longitudinal magnetizations to be at or close to the null point [90]. Adiabatic inversion recovery (AIR) UTE (AIR-UTE) [94,95] is similar to the abovementioned IR-UTE technique in its ability to visualize bound water in cortical bone and provide a qualitative image of cortical bone structure. Dual-adiabatic inversion recovery (Dual-IR) sequences (two long IR pulses used successively at long T2 water and long T2 fat frequencies, respectively [92,96,97]) or double inversion recovery (Double-IR) UTE sequences (two identical IR pulses with a center frequency located at the water peak, but the spectral width is broad enough to cover both water and fat frequencies [98]) can also be employed to invert and null signals from long T2 water and fat, respectively [92]. The IR-UTE-based qualitative bone imaging sequence has been applied to different bone sites in vivo; however, the contrast and image quality depend on the anatomical location, coil quality and size, bone thickness and so on. Water and fat-suppressed proton projection MRI (WASPI) is another MRI sequence developed for selective imaging of bone water bound to the organic matrix [99–101]. WASPI uses dual hard pulses with narrow frequency bands to selectively excite the water and fat signals, followed by strong gradient crushers that saturate the free water and fat signals before data acquisition [99]. Since bound water has a short T2*, it will remain largely unsaturated and provide qualitative imaging of bound water in bone [102]. Besides the discussed UTE MRI techniques, Zero echo time (ZTE) sequence has also been used for cortical bone imaging, which employs a short rectangular excitation pulse during the fully ramped up readout gradient, followed by fast radial sampling [103,104]. Alternatively, frequency-modulated pulse with interleaved transmit-receive operation, known

Author Manuscript Author Manuscript Author Manuscript Author Manuscript

as sweep imaging with Fourier transformation (SWIFT) can also be used for bone imaging [105].

Direct trabecular bone imaging has been pursued using WASPI and fat-suppressed UTE techniques [106–108]. To create a high contrast for trabecular bone in proton imaging, it is critical to suppress signals from tissues with long T2 relaxation times, particularly the free water and fat in bone marrow. Ma et al. [109] have proposed a 3D adiabatic IR-UTE Cones (3D IR-UTE-Cones) sequence to directly visualize trabecular bone. Their technique uses a broadband adiabatic inversion pulse together with a short repetition time to inversion time (TR/TI) ratio to suppress signals from tissues with long T2 relaxation times such as muscle and marrow fat.

Performing FEA-based studies using the described direct bone imaging techniques could be a major step towards more accurate assessment of bone competence and surely calls for future scientific effort and investigation. It will be beneficial to develop FE models using a combination of direct and indirect bone imaging for cortical bone and trabecular bone sites, respectively. Following such a combination, sub-voxel cortical bone porosity could be considered in the model while avoiding the challenges for direct bone imaging at trabecular bone sites. Combining direct and indirect trabecular bone imaging will be challenging due to potential mismatches in image resolutions, difficulties in image registration required for motion compensation, complications in bone segmentation, and boundary condition definition.

4. Limitations and challenges

MRI-based micro-FEA has demonstrated potential for assessment of mechanical competence based on trabecular bone structure. MRI-based techniques avoid potential harm from ionizing radiation, and simultaneously obtain complementary information from bone and surrounding soft tissues. However, MRI-based micro-FEA still requires comprehensive validation and verification studies before being translated to clinical investigations. Only a few studies to date have validated MRI-based FE models by comparing their results with μCT-based FE models as a reference [40,44,68]. However, a comprehensive verification and validation process whereby FEA results are compared with those obtained from experimental mechanical tests is required for any specific FE model, including its hypothesized failure criteria, boundary conditions, imaging protocol, and meshing. To the authors' knowledge, the only reported validation for MRI-based micro-FEA has been recently performed by Rajapakse et el., [30] on cadaveric distal tibiae simulating compression loading. Future validation investigations should also be performed on more critical bone sites with higher prevalence of osteoporotic fractures such as the proximal femur and spine.

The results of the FE models largely depend on the material properties assigned to the elements of the model. Similar elastic values as those used in CT-based studies could also be used for MRI data if bone structure is binarized and if segmented bone voxels between the modalities are similar. Using element material properties as a function of MRI signal (i.e., BVF) is another approach, but the relationship between BVF signal and microscale

Author Manuscript Author Manuscript Author Manuscript Author Manuscript

mechanical properties has not been fully validated. In future studies, this could be achieved by performing mechanical indentation tests at different bone sites at the trabecular level or by performing four-point bending tests on cortical bone strips. Such relationships should be examined for the various MRI techniques used for FEA studies, as the different MRI parameters may result in significantly altered bone signal and contrast levels. The pairing of direct MR imaging and micro-FEA of bone also requires comprehensive validation to elucidate the relationship between bound water proton density and the elastic modulus at the element-level. It should be noted that reaching a consensus on the microscale mechanical and MRI signal relationship will be challenging as such agreement is yet to be achieved even on pure experimental elastic modulus, with reported values ranging from 5 to 24 GPa [17].

In addition to the validation requirements, there are other major limitations to the widespread use of MRI-based micro-FEA studies. This includes the long scan times required for MR image acquisition compared to x-ray-based methods, resulting in potential motion-related artifacts, and the associated high costs for MRI, limiting its availability in some populations. The combination of advanced MRI acceleration techniques to further shorten the scan time with hardware developments resulting in more affordable MRI scanners for musculoskeletal targets will help with improving patient access.

5. Conclusions

This review study summarizes steps for linear and non-linear FEA derived from bone MRI images to predict bone mechanical competence as a potential non-invasive bone fracture risk estimation with no ionizing radiation. MRI-based FEA investigations and the corresponding MRI sequences have been described. FEA studies based on indirect bone imaging dominates this field of research. Future potential pathways to more accurate MRI-based models via direct bone imaging have been discussed for investigation in future studies.

Acknowledgements

The authors acknowledge grant support from NIH (R01AR075825, 1R01NS092650, R01AR062581-06) and VA Clinical Science and Rehabilitation R&D Awards (I01CX001388 and I01RX002604).

8. References:

[1]. Zanker J, Duque G. Osteoporosis in Older Persons: Old and New Players. J Am Geriatr Soc 2019;67:831–40. 10.1111/jgs.15716. [PubMed: 30570741]

[2]. Guerri S, Mercatelli D, Gómez MPA, Napoli A, Battista G, Guglielmi G, et al. Quantitative imaging techniques for the assessment of osteoporosis and sarcopenia. Quant Imaging Med Surg 2018;8:60–85. 10.21037/qims.2018.01.05. [PubMed: 29541624]

[3]. Looker AC, Frenk SM. Percentage of Adults Aged 65 and Over With Osteoporosis or Low Bone Mass at the Femur Neck or Lumbar Spine: United States, 2005–2010. Centers Dis Control Prev 2015:2005–10.

[4]. Yeni YN, Brown CU, Norman TL. Influence of bone composition and apparent density on fracture toughness of the human femur and tibia. Bone 1998. 10.1016/S8756-3282(97)00227-5.

[5]. De Laet CEDH Van Hout BA, Burger H, Hofman A, Pols HAP. Bone density and risk of hip fracture in men and women: Cross sectional analysis. Br Med J 1997;315:11–5. 10.1136/bmj.315.7102.221.

Author Manuscript Author Manuscript Author Manuscript Author Manuscript

[6]. Trajanoska K, Schoufour JD, de Jonge EAL, Kieboom BCT, Mulder M, Stricker BH, et al. Fracture incidence and secular trends between 1989 and 2013 in a population based cohort: The Rotterdam Study. Bone 2018;114:116–24. 10.1016/j.bone.2018.06.004. [PubMed: 29885926]

[7]. Cummings SR. Are patients with hip fractures more osteoporotic? Review of Evidence. Am J Med 1985;8:487–94.

[8]. Marshall D, Johnell O, Wedel H. Meta-analysis of how well measures of bone mineral density predict occurrence of osteoporotic fractures. Br Med J 1996;18:1254–9. 10.1136/bmj.312.7041.1254.

[9]. Faulkner KG. Bone Matters: Are Density Increases Necessary to Reduce Fracture Risk? J Bone Miner Res 2000;15:183–7. 10.1359/jbmr.2000.15.2.183. [PubMed: 10703919]

[10]. Schuit SCE, Van Der Klift M, Weel AEAM, De Laet CEDH, Burger H, Seeman E, et al. Fracture incidence and association with bone mineral density in elderly men and women: The Rotterdam Study. Bone 2004;34:195–202. 10.1016/j.bone.2003.10.001. [PubMed: 14751578]

[11]. Sandor T, Felsenberg D, Brown E. Comments on the hypotheses underlying fracture risk assessment in osteoporosis as proposed by the World Health Organization. Calcif Tissue Int 1999. 10.1007/s002239900616.

[12]. McCreadie BR, Goldstein SA. Biomechanics of fracture: Is bone mineral density sufficient to assess risk? J Bone Miner Res 2000. 10.1359/jbmr.2000.15.12.2305.

[13]. Homminga J, McCreadie BR, Ciarelli TE, Weinans H, Goldstein SA, Huiskes R. Cancellous bone mechanical properties from normals and patients with hip fractures differ on the structure level, not on the bone hard tissue level. Bone 2002. 10.1016/S8756-3282(02)00693-2.

[14]. Kanis JA, Johnell O, Oden A, Dawson A, De Laet C, Jonsson B. Ten year probabilities of osteoporotic fractures according to BMD and diagnostic thresholds. Osteoporos Int 2001. 10.1007/s001980170006.

[15]. Russo CR, Lauretani F, Bandinelli S, Bartali B, Di Iorio A, Volpato S, et al. Aging bone in men and women: Beyond changes in bone mineral density. Osteoporos Int 2003. 10.1007/s00198-002-1322-y.

[16]. Kanis JA, Johnell O, Oden A, Johansson H, McCloskey E. FRAX™ and the assessment of fracture probability in men and women from the UK. Osteoporos Int 2008;19:385–97. 10.1007/s00198-007-0543-5. [PubMed: 18292978]

[17]. Oftadeh R, Perez-Viloria M, Villa-Camacho JC, Vaziri A, Nazarian A. Biomechanics and Mechanobiology of Trabecular Bone: A Review. J Biomech Eng 2015;137:1–15. 10.1115/1.4029176.

[18]. Novitskaya E, Chen P-Y, Hamed E, Jun L, Lubarda V, Jasiuk I, et al. Recent advances on the measurement and calculation of the elastic moduli of cortical and trabecular bone: A review. Theor Appl Mech 2011;38:209–97. 10.2298/TAM1103209N.

[19]. Ulrich D, Van Rietbergen B, Laib A, R̈uegsegger P. The ability of three-dimensional structural indices to reflect mechanical aspects of trabecular bone. Bone 1999. 10.1016/S8756-3282(99)00098-8.

[20]. Engelke K, van Rietbergen B, Zysset P. FEA to Measure Bone Strength: A Review. Clin Rev Bone Miner Metab 2016;14:26–37. 10.1007/s12018-015-9201-1.

[21]. Einafshar M, Hashemi A, van Lenthe GH. Homogenized finite element models can accurately predict screw pull-out in continuum materials, but not in porous materials. Comput Methods Programs Biomed 2021;202. 10.1016/j.cmpb.2021.105966.

[22]. Nazarian A, Stauber M, Zurakowski D, Snyder BD, Müller R. The interaction of microstructure and volume fraction in predicting failure in cancellous bone. Bone 2006;39:1196–202. 10.1016/j.bone.2006.06.013. [PubMed: 16920051]

[23]. Metzger CE, Burr DB, Allen MR. Anatomy and Structural Considerations. In: Zaidi MBT-E of BB, editor. Encycl. Bone Biol, Oxford: Academic Press; 2020, p. 218–32. 10.1016/B978-0-12-801238-3.62234-1.

[24]. Podshivalov L, Fischer A, Bar-Yoseph PZ. 3D hierarchical geometric modeling and multiscale FE analysis as a base for individualized medical diagnosis of bone structure. Bone 2011;48:693–703. 10.1016/j.bone.2010.12.022. [PubMed: 21193070]

Author Manuscript Author Manuscript Author Manuscript Author Manuscript

[25]. Podshivalov L, Fischer A, Bar-Yoseph PZ. Multiscale FE method for analysis of bone micro-structures. J Mech Behav Biomed Mater 2011;4:888–99. 10.1016/j.jmbbm.2011.03.003. [PubMed: 21616470]

[26]. Zhang N, Magland JF, Rajapakse CS, Bhagat YA, Wehrli FW. Potential of in vivo MRI-based nonlinear finite-element analysis for the assessment of trabecular bone post-yield properties. Med Phys 2013;40:1–10. 10.1118/1.4802085.

[27]. Zhang N, Magland JF, Rajapakse CS, Lam SCB, Wehrli FW. Assessment of Trabecular Bone Yield and Post-yield Behavior from High-Resolution MRI-Based Nonlinear Finite Element Analysis at the Distal Radius of Premenopausal and Postmenopausal Women Susceptible to Osteoporosis. Acad Radiol 2013;20:1584–91. 10.1016/j.acra.2013.09.005. [PubMed: 24200486]

[28]. Rajapakse CS, Magland JF, Wald MJ, Liu XS, Zhang XH, Guo XE, et al. Computational biomechanics of the distal tibia from high-resolution MR and micro-CT images. Bone 2010;47:556–63. 10.1016/j.bone.2010.05.039. [PubMed: 20685323]

[29]. Ladd AJC, Kinney JH, Haupt DL, Goldstein SA. Finite-element modeling of trabecular bone: Comparison with mechanical testing and determination of tissue modulus. J Orthop Res 1998;16:622–8. 10.1002/jor.1100160516. [PubMed: 9820288]

[30]. Rajapakse CS, Kobe EA, Batzdorf AS, Hast MW, Wehrli FW. Accuracy of MRI-based finite element assessment of distal tibia compared to mechanical testing. Bone 2018;108:71–8. 10.1016/j.bone.2017.12.023. [PubMed: 29278746]

[31]. Rajapakse CS, Hotca A, Newman BT, Ramme A, Vira S, Kobe EA, et al. Patient-specific Hip Fracture Strength Assessment with Microstructural MR Imaging-based Finite Element Modeling. Radiology 2017;283:854–61. [PubMed: 27918708]

[32]. Majumdar S Noninvasive assessment of trabecular bone architecture and the competence of bone: Preface. Adv. Exp. Med. Biol, 2001.

[33]. Nazarian A, Müller R. Time-lapsed microstructural imaging of bone failure behavior. J Biomech 2004;37:55–65. 10.1016/S0021-9290(03)00254-9. [PubMed: 14672568]

[34]. MacNeil JA, Boyd SK. Accuracy of high-resolution peripheral quantitative computed tomography for measurement of bone quality. Med Eng Phys 2007;29:1096–105. 10.1016/j.medengphy.2006.11.002. [PubMed: 17229586]

[35]. van Rietbergen B, Odgaard A, Kabel J, Huiskes R. Direct mechanics assessment of elastic symmetries and properties of trabecular bone architecture. J Biomech 1996;29:1653–7. [PubMed: 8945668]

[36]. Bevill G, Keaveny TM. Trabecular bone strength predictions using finite element analysis of micro-scale images at limited spatial resolution. Bone 2009;44:579–84. 10.1016/j.bone.2008.11.020. [PubMed: 19135184]

[37]. Orwoll ES, Marshall LM, Nielson CM, Cummings SR, Lapidus J, Cauley JA, et al. Finite element analysis of the proximal femur and hip fracture risk in older men. J Bone Miner Res 2009;24:475–83. 10.1359/jbmr.081201. [PubMed: 19049327]

[38]. Keyak JH, Sigurdsson S, Karlsdottir GS, Oskarsdottir D, Sigmarsdottir A, Kornak J, et al. Effect of finite element model loading condition on fracture risk assessment in men and women: The AGES-Reykjavik study. Bone 2013;57:18–29. 10.1016/j.bone.2013.07.028. [PubMed: 23907032]

[39]. Damilakis J, Adams JE, Guglielmi G, Link TM. Radiation exposure in X-ray-based imaging techniques used in osteoporosis. Eur Radiol 2010;20:2707–14. 10.1007/s00330-010-1845-0. [PubMed: 20559834]

[40]. Van Rietbergen B, Majumdar S, Pistoia W, Newitt DC, Kothari M, Laib A, et al. Assessment of cancellous bone mechanical properties from micro-FE models based on micro-CT, pQCT and MR images. Technol Heal Care 1998;6:413–20. 10.3233/thc-1998-65-613.

[41]. Newitt DC, Majumdar S, Van Rietbergen B, Von Ingersleben G, Harris ST, Genant HK, et al. In vivo assessment of architecture and micro-finite element analysis derived indices of mechanical properties of trabecular bone in the radius. Osteoporos Int 2002;13:6–17. 10.1007/s198-002-8332-0. [PubMed: 11878456]

[42]. Newitt DC, Van Rietbergen B, Majumdar S. Processing and analysis of in vivo high-resolution MR images of trabecular bone for longitudinal studies: Reproducibility of structural measures

Author Manuscript Author Manuscript Author Manuscript Author Manuscript

and micro-finite element analysis derived mechanical properties. Osteoporos Int 2002;13:278–87. 10.1007/s001980200027. [PubMed: 12030542]

[43]. Van Rietbergen B, Majumdar S, Newitt D, MacDonald B. High-resolution MRI and micro-FE for the evaluation of changes in bone mechanical properties during longitudinal clinical trials: Application to calcaneal bone in postmenopausal women after one year of idoxifene treatment. Clin Biomech 2002;17:81–8. 10.1016/S0268-0033(01)00110-3.

[44]. Rajapakse CS, Magland J, Zhang H, Liu XS, Wehrli SL, Guo XE, et al. Implications of noise and resolution on mechanical properties of trabecular bone estimated by image-based finite-element analysis. J Orthop Res 2009;27:1263–71. 10.1002/jor.20877. [PubMed: 19338030]

[45]. Majumdar S Magnetic resonance imaging of trabecular bone structure. Top Magn Reson Imaging 2002;13:323–34. 10.1097/00002142-200210000-00004. [PubMed: 12464745]

[46]. Wehrli FW. Structural and functional assessment of trabecular and cortical bone by micro magnetic resonance imaging. J Magn Reson Imaging 2007;25:390–409. 10.1002/jmri.20807. [PubMed: 17260403]

[47]. Chang G, Deniz CM, Honig S, Rajapakse CS, Egol K, Regatte RR, et al. Feasibility of three-dimensional MRI of proximal femur microarchitecture at 3 tesla using 26 receive elements without and with parallel imaging. J Magn Reson Imaging 2014;40:229–38. 10.1002/jmri.24345. [PubMed: 24711013]

[48]. Han M, Chiba K, Banerjee S, Carballido-Gamio J, Krug R. Variable flip angle three-dimensional fast spin-echo sequence combined with outer volume suppression for imaging trabecular bone structure of the proximal femur. J Magn Reson Imaging 2015;41:1300–10. 10.1002/jmri.24673. [PubMed: 24956149]

[49]. Li X, Kuo D, Schafer AL, Porzig A, Link TM, Black D, et al. Quantification of vertebral bone marrow fat content using 3 Tesla MR spectroscopy: Reproducibility, vertebral variation, and applications in osteoporosis. J Magn Reson Imaging 2011;33:974–9. 10.1002/jmri.22489. [PubMed: 21448966]

[50]. Mostoufi-Moab S, Magland J, Isaacoff EJ, Sun W, Rajapakse CS, Zemel B, et al. Adverse fat depots and marrow adiposity are associated with skeletal deficits and insulin resistance in long-term survivors of pediatric hematopoietic stem cell transplantation. J Bone Miner Res 2015;30:1657–66. 10.1002/jbmr.2512. [PubMed: 25801428]

[51]. Jerban S, Ma Y, Namiranian B, Ashir A, Shirazian H, Zhao W, et al. Age-related decrease in collagen proton fraction in tibial tendons estimated by magnetization transfer modeling of ultrashort echo time magnetic resonance imaging (UTE-MRI). Sci Rep 2019;November:17974. 10.1038/s41598-019-54559-3. [PubMed: 31784631]

[52]. Chang EY, Du J, Chung CB. UTE imaging in the musculoskeletal system. J Magn Reson Imaging 2015;41:870–83. 10.1002/jmri.24713. [PubMed: 25045018]

[53]. Wehrli FW, Song HK, Saha PK, Wright AC. Quantitative MRI for the assessment of bone structure and function. NMR Biomed 2006;19:731–64. 10.1002/nbm. [PubMed: 17075953]

[54]. Sharma AK, Toussaint ND, Elder GJ, Masterson R, Holt SG, Robertson PL, et al. Magnetic resonance imaging based assessment of bone microstructure as a non-invasive alternative to histomorphometry in patients with chronic kidney disease. Bone 2018;114:14–21. 10.1016/j.bone.2018.05.029. [PubMed: 29860153]

[55]. Du J, Hermida JC, Diaz E, Corbeil J, Znamirowski R, D'Lima DD, et al. Assessment of cortical bone with clinical and ultrashort echo time sequences. Magn Reson Med 2013;70:697–704. 10.1002/mrm.24497. [PubMed: 23001864]

[56]. Vasilic B, Wehrli FW. A novel local thresholding algorithm for trabecular bone volume fraction mapping in the limited spatial resolution regime of in vivo MRI. IEEE Trans Med Imaging 2005;24:1574–85. 10.1109/TMI.2005.859192. [PubMed: 16353372]

[57]. Magland JF, Zhang N, Rajapakse CS, Wehrli FW. Computationally-optimized bone mechanical modeling from high-resolution structural images. PLoS One 2012;7:e35525. 10.1371/journal.pone.0035525. [PubMed: 22558164]

[58]. Rajapakse CS, Magland JF, Wald MJ, Liu XS, Zhang XH, Guo XE, et al. Computational Biomechanics of the Distal Tibia from High Resolution MR and Micro-CT Images. Bone 2010;47:556–563. 10.1016/j.bone.2010.05.039. [PubMed: 20685323]

Author Manuscript Author Manuscript Author Manuscript Author Manuscript

[59]. Bouxsein ML, Boyd SK, Christiansen BA, Guldberg RE, Jepsen KJ, Müller R. Guidelines for assessment of bone microstructure in rodents using micro-computed tomography. J Bone Miner Res 2010;25:1468–86. 10.1002/jbmr.141. [PubMed: 20533309]

[60]. Fritsch A, Hellmich C. “Universal” microstructural patterns in cortical and trabecular, extracellular and extravascular bone materials: Micromechanics-based prediction of anisotropic elasticity. J Theor Biol 2007;244:597–620. 10.1016/j.jtbi.2006.09.013. [PubMed: 17074362]

[61]. Ritchie RO, Buehler MJ, Hansma P. Plasticity and toughness in bone. Phys Today 2009;62:41–7. 10.1063/1.3156332.

[62]. Alberich-Bayarri A, Marti-Bonmati L, Sanz-Requena R, Belloch E, Moratal D. In vivo trabecular bone morphologic and mechanical relationship using high-resolution 3-T MRI. Am J Roentgenol 2008;191:721–6. 10.2214/AJR.07.3528. [PubMed: 18716099]

[63]. Rajapakse CS, Leonard MB, Bhagat YA, Sun W, Magland JF, Wehrli FW. Micro-MR imaging-based computational biomechanics demonstrates reduction in cortical and trabecular bone strength after renal transplantation. Radiology 2012;262:912–20. 10.1148/radiol.11111044. [PubMed: 22357891]

[64]. Pistoia W, Van Rietbergen B, Lochmüller EM, Lill CA, Eckstein F, Rüegsegger P. Estimation of distal radius failure load with micro-finite element analysis models based on three-dimensional peripheral quantitative computed tomography images. Bone 2002;30:842–8. 10.1016/S8756-3282(02)00736-6. [PubMed: 12052451]

[65]. Mueller TL, Christen D, Sandercott S, Boyd SK, van Rietbergen B, Eckstein F, et al. Computational finite element bone mechanics accurately predicts mechanical competence in the human radius of an elderly population. Bone 2011;48:1232–8. 10.1016/j.bone.2011.02.022. [PubMed: 21376150]

[66]. Keyak JH. Improved prediction of proximal femoral fracture load using nonlinear finite element models. Med Eng Phys 2001;23:165–73. 10.1016/S1350-4533(01)00045-5. [PubMed: 11410381]

[67]. Patton DM, Bigelow EMR, Schlecht SH, Kohn DH, Bredbenner TL, Jepsen KJ. The relationship between whole bone stiffness and strength is age and sex dependent. J Biomech 2019;83:125–33. 10.1016/j.jbiomech.2018.11.030. [PubMed: 30527634]

[68]. Liu XS, Zhang XH, Rajapakse CS, Wald MJ, Magland J, Sekhon KK, et al. Accuracy of high-resolution in vivo micro magnetic resonance imaging for measurements of microstructural and mechanical properties of human distal tibial bone. J Bone Miner Res 2010;25:2039–50. 10.1002/jbmr.92. [PubMed: 20499379]

[69]. Wehrli FW, Rajapakse CS, Magland JF, Snyder PJ. Mechanical implications of estrogen supplementation in early postmenopausal women. J Bone Miner Res 2010;25:1406–14. 10.1002/jbmr.33. [PubMed: 20200948]

[70]. Chang G, Rajapakse CS, Babb JS, Honig SP, Recht MP, Regatte RR. In vivo estimation of bone stiffness at the distal femur and proximal tibia using ultra-high-field 7-Tesla magnetic resonance imaging and micro-finite element analysis. J Bone Miner Metab 2012;30:243–51. 10.1007/s00774-011-0333-1. [PubMed: 22124539]

[71]. Chang G, Rajapakse CS, Diamond M, Honig S, Recht MP, Weiss DS, et al. Micro-finite element analysis applied to high-resolution MRI reveals improved bone mechanical competence in the distal femur of female pre-professional dancers. Osteoporos Int 2013;24:1407–17. 10.1007/s00198-012-2105-8. [PubMed: 22893356]

[72]. Chang G, Honig S, Brown R, Deniz CM, Egol KA, Babb JS, et al. Finite element analysis applied to 3-T MR imaging of proximal femur microarchitecture: Lower bone strength in patients with fragility fractures compared with control subjects. Radiology 2014;272:464–74. 10.1148/radiol.14131926. [PubMed: 24689884]

[73]. Chang G, Hotca-Cho A, Rusinek H, Honig S, Mikheev A, Egol K, et al. Measurement reproducibility of magnetic resonance imaging-based finite element analysis of proximal femur microarchitecture for in vivo assessment of bone strength. Magn Reson Mater Physics, Biol Med 2015;28:407–12. 10.1007/s10334-014-0475-y.

[74]. Cowin SC. Bone poroelasticity. J Biomech 1999;32:217–38. 10.1016/S0021-9290(98)00161-4. [PubMed: 10093022]

Author Manuscript Author Manuscript Author Manuscript Author Manuscript

[75]. Wang X, Ni Q. Determination of cortical bone porosity and pore size distribution using a low field pulsed NMR approach. J Orthop Res 2003;21:312–9. 10.1016/S0736-0266(02)00157-2. [PubMed: 12568964]

[76]. Jerban S, Ma Y, Wong JHJHJH, Nazaran A, Searleman A, Wan L, et al. Ultrashort echo time magnetic resonance imaging (UTE-MRI) of cortical bone correlates well with histomorphometric assessment of bone microstructure. Bone 2019;123:8–17. 10.1016/j.bone.2019.03.013. [PubMed: 30877070]

[77]. Rajapakse CS, Bashoor-Zadeh M, Li C, Sun W, Wright AC, Wehrli FW. Volumetric Cortical Bone Porosity Assessment with MR Imaging: Validation and Clinical Feasibility. Radiology 2015;276:526–35. 10.1148/radiol.15141850. [PubMed: 26203710]

[78]. Jerban S, Ma Y, Li L, Jang H, Wan L, Guo T, et al. Volumetric Mapping of Bound and Pore Water as well as Collagen Protons in Cortical Bone Using 3D Ultrashort Echo Time Cones MR Imaging Techniques. Bone 2019;127:120–8. 10.1016/j.bone.2019.05.038. [PubMed: 31176044]

[79]. Manhard MK, Uppuganti S, Granke M, Gochberg DF, Nyman JS, Does MD. MRI-derived bound and pore water concentrations as predictors of fracture resistance. Bone 2016;87:1–10. 10.1016/j.bone.2016.03.007. [PubMed: 26993059]

[80]. Ma Y-J, Jerban S, Jang H, Chang D, Chang EY, Du J. Quantitative Ultrashort Echo Time (UTE) Magnetic Resonance Imaging of Bone: An Update. Front Endocrinol (Lausanne) 2020;11:667–76. 10.3389/fendo.2020.56741.

[81]. Jerban S, Lu X, Dorthe EWEW, Alenezi S, Ma Y, Kakos L, et al. Correlations of cortical bone microstructural and mechanical properties with water proton fractions obtained from ultrashort echo time (UTE) MRI tricomponent T2* model. NMR Biomed 2020;33:e4233. 10.1002/nbm.4233. [PubMed: 31820518]

[82]. Robson MD, Gatehouse PD, Bydder M, Bydder GM. Magnetic Resonance: An Introduction to Ultrashort TE (UTE) Imaging. J Comput Assist Tomogr 2003;27:825–46. 10.1097/00004728-200311000-00001. [PubMed: 14600447]

[83]. Ho KY, Keyak JH, Powers CM. Comparison of patella bone strain between females with and without patellofemoral pain: A finite element analysis study. J Biomech 2014;47:230–6. 10.1016/j.jbiomech.2013.09.010. [PubMed: 24188973]

[84]. Jerban S, Chang DG, Ma Y, Jang H, Chang EY, Du J. An Update in Qualitative Imaging of Bone Using Ultrashort Echo Time Magnetic Resonance. Front Endocrinol (Lausanne) 2020;11:677–89. 10.3389/fendo.2020.555756.

[85]. Jerban S, Ma Y, Wei Z, Jang H, Chang EY, Du J. Quantitative Magnetic Resonance Imaging of Cortical and Trabecular Bone. Semin Musculoskelet Radiol 2020;24:386–401. 10.1055/s-0040-1710355. [PubMed: 32992367]

[86]. Du J, Bydder GM. Qualitative and quantitative ultrashort-TE MRI of cortical bone. NMR Biomed 2013;26:489–506. 10.1002/nbm.2906. [PubMed: 23280581]

[87]. Li C, Seifert AC, Rad HS, Bhagat Y a, Rajapakse CS, Sun W, et al. Cortical Bone Water Concentration: Dependence of MR Imaging Measures on Age and Pore Volume Fraction. Radiology 2014;272:796–806. 10.1148/radiol.14132585. [PubMed: 24814179]

[88]. Du J, Bydder M, Takahashi AM, Carl M, Chung CB, Bydder GM. Short T2 contrast with three-dimensional ultrashort echo time imaging. Magn Reson Imaging 2011;29:470–82. 10.1016/j.mri.2010.11.003. [PubMed: 21440400]

[89]. Reichert ILH, Robson MD, Gatehouse PD, He T, Chappell KE, Holmes J, et al. Magnetic resonance imaging of cortical bone with ultrashort TE pulse sequences. Magn Reson Imaging 2005;23:611–8. 10.1016/j.mri.2005.02.017. [PubMed: 16051035]

[90]. Du J, Bydder M, Takahashi AM, Chung CB. Two-dimensional ultrashort echo time imaging using a spiral trajectory. Magn Reson Imaging 2008;26:304–12. 10.1016/j.mri.2007.08.005. [PubMed: 18096346]

[91]. Du J, Takahashi AM, Chung CB. Ultrashort TE spectroscopic imaging (UTESI): Application to the imaging of short T2 relaxation tissues in the musculoskeletal system. J Magn Reson Imaging 2009;29:412–21. 10.1002/jmri.21465. [PubMed: 19161197]

Author Manuscript Author Manuscript Author Manuscript Author Manuscript

[92]. Du J, Takahashi AM, Bae WC, Chung CB, Bydder GM. Dual inversion recovery, ultrashort echo time (DIR UTE) imaging: Creating high contrast for short-T2species. Magn Reson Med 2010;63:447–55. 10.1002/mrm.22257. [PubMed: 20099332]

[93]. Nazaran A, Carl M, Ma Y, Jerban S, Lu X, Du J, et al. Three-dimensional adiabatic inversion recovery prepared ultrashort echo time cones (3D IR-UTE-Cones) imaging of cortical bone in the hip. Magn Reson Imaging 2017;44:60–4. 10.1016/j.mri.2017.07.012. [PubMed: 28716680]

[94]. Nyman JS, Gorochow LE, Adam Horch R, Uppuganti S, Zein-Sabatto A, Manhard MK, et al. Partial removal of pore and loosely bound water by low-energy drying decreases cortical bone toughness in young and old donors. J Mech Behav Biomed Mater 2013;22:136–45. 10.1016/j.jmbbm.2012.08.013. [PubMed: 23631897]

[95]. Manhard MK, Horch RA, Gochberg DF, Nyman JS, Does MD. In Vivo Quantitative MR Imaging of Bound and Pore Water in cortical bone. Radiology 2015;277:221–30. [PubMed: 26020434]

[96]. Du J, Carl M, Bae WC, Statum S, Chang EY, Bydder GM, et al. Dual inversion recovery ultrashort echo time (DIR-UTE) imaging and quantification of the zone of calcified cartilage (ZCC). Osteoarthr Cartil 2013;21:77–85. 10.1016/j.joca.2012.09.009.

[97]. Garwood M, DelaBarre L. The return of the frequency sweep: Designing adiabatic pulses for contemporary NMR. J Magn Reson 2001;153:155–77. 10.1006/jmre.2001.2340. [PubMed: 11740891]

[98]. Ma YJ, Zhu Y, Lu X, Carl M, Chang EY, Du J. Short T 2 imaging using a 3D double adiabatic inversion recovery prepared ultrashort echo time cones (3D DIR-UTE-Cones) sequence. Magn Reson Med 2017;00:1–9. 10.1002/mrm.26908.

[99]. Wu Y, Ackerman JL, Chesler DA, Graham L, Wang Y, Glimcher MJ. Density of organic matrix of native mineralized bone measured by water and fat-suppressed proton projection MRI. Magn Reson Med 2003;50:59–68. 10.1002/mrm.10512. [PubMed: 12815679]

[100]. Cao H, Ackerman JL, Hrovat MI, Graham L, Glimcher MJ, Wu Y. Quantitative bone matrix density measurement by water and fat-suppressed proton projection MRI (WASPI) with polymer calibration phantoms. Magn Reson Med 2008. 10.1002/mrm.21771.

[101]. Cao H, Nazarian A, Ackerman JL, Snyder BD, Rosenberg AE, Nazarian RM, et al. Quantitative 31P NMR spectroscopy and 1H MRI measurements of bone mineral and matrix density differentiate metabolic bone diseases in rat models. Bone 2010;46:1582–90. 10.1016/j.bone.2010.02.020. [PubMed: 20188225]

[102]. Wu Y, Hrovat MI, Ackerman JL, Reese TG, Cao H, Ecklund K, et al. Bone matrix imaged in vivo by water and fat-suppressed proton projection MRI (WASPI) of animal and human subjects. J Magn Reson Imaging 2010;31:954–63. 10.1002/jmri.22130. [PubMed: 20373441]

[103]. Breighner RE, Endo Y, Konin GP, Gulotta LV., Koff MF, Potter HG. Zero echo time imaging of the shoulder: Enhanced osseous detail by using MR imaging. Radiology 2018;286:960–6. 10.1148/radiol.2017170906. [PubMed: 29117482]

[104]. Weiger M, Pruessmann KP. MRI with Zero Echo Time. Encycl Magn Reson 2012;1:311–22. 10.1002/9780470034590.emrstm1292.

[105]. Garwood M, Idiyatullin D, Corum CA, Chamberlain R, Moeller S, Kobayashi N, et al. Capturing Signals from Fast-relaxing Spins with Frequency-Swept MRI: SWIFT. Encycl Magn Reson 2012;1:322–32. 10.1002/9780470034590.emrstm1259.

[106]. Wu Y, Dai G, Ackerman JL, Hrovat MI, Glimcher MJ, Snyder BD, et al. Water and fat-suppressed proton projection MRI (WASPI) of rat femur bone. Magn Reson Med 2007;57:554–67. 10.1002/mrm.21174. [PubMed: 17326184]

[107]. Weiger M, Stampanoni M, Pruessmann KP. Direct depiction of bone microstructure using MRI with zero echo time. Bone 2013;54:44–7. 10.1016/j.bone.2013.01.027. [PubMed: 23356986]

[108]. Wurnig MC, Calcagni M, Kenkel D, Vich M, Weiger M, Andreisek G, et al. Characterization of trabecular bone density with ultra-short echo-time MRI at 1.5, 3.0 and 7.0 T comparison with micro-computed tomography. NMR Biomed 2014;27:1159–66. 10.1002/nbm.3169. [PubMed: 25088271]

[109]. Ma YJ, Chen Y, Li L, Cai Z, Wei Z, Jerban S, et al. Trabecular bone imaging using a 3D adiabatic inversion recovery prepared ultrashort TE Cones sequence at 3T. Magn Reson Med 2020;83:1640–51. 10.1002/mrm.28027. [PubMed: 31631404]

Author Manuscript Author Manuscript Author Manuscript Author Manuscript

[110]. Magland J, Vasilic B, Wehrli F. Fast low-angle dual spin-echo (FLADE): A new robust pulse sequence for structural imaging of trabecular bone. Magn Reson Med 2006;55:465–71. 10.1002/mrm.20789. [PubMed: 16463354]

[111]. Techawiboonwong A, Song HK, Magland JF, Saha PK, Wehrli FW. Implications of pulse sequence in structural imaging of trabecular bone. J Magn Reson Imaging 2005;22:647–55. 10.1002/jmri.20432. [PubMed: 16215967]

Author Manuscript Author Manuscript Author Manuscript Author Manuscript

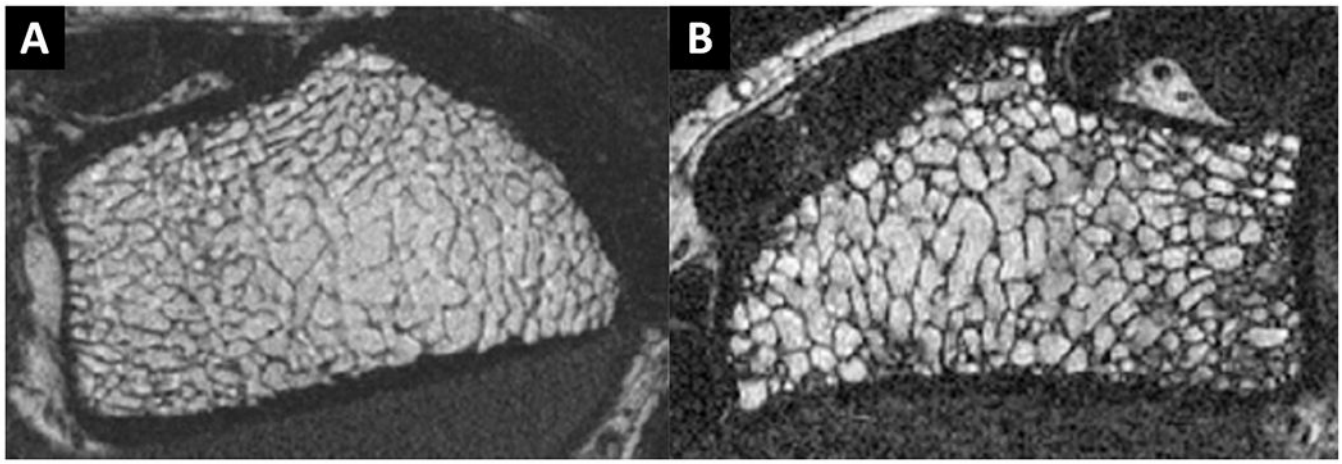

Figure 1.

Visualized trabecular bone as dark regions surrounded by bright marrow using two different 3D MRI sequences performed on the distal radius at 1.5T. (A) Fast large-angle spin-echo, FLASE (scan time: 11.5 min, voxel size = 137×137×410 μm) [46,110]. (B) balanced steady-state free precession, bSSSP (scan time: 4 min, voxel size ≈ 0.16×0.16×0.5mm) [46,111]. These figures were previously presented by Magland et al. [110], Techawiboonwong et al. [111], and Wehrli et al. [46]. Reprinting permission is granted through Rightslink. Minor modifications were performed for presentation purposes.

Author Manuscript Author Manuscript Author Manuscript Author Manuscript

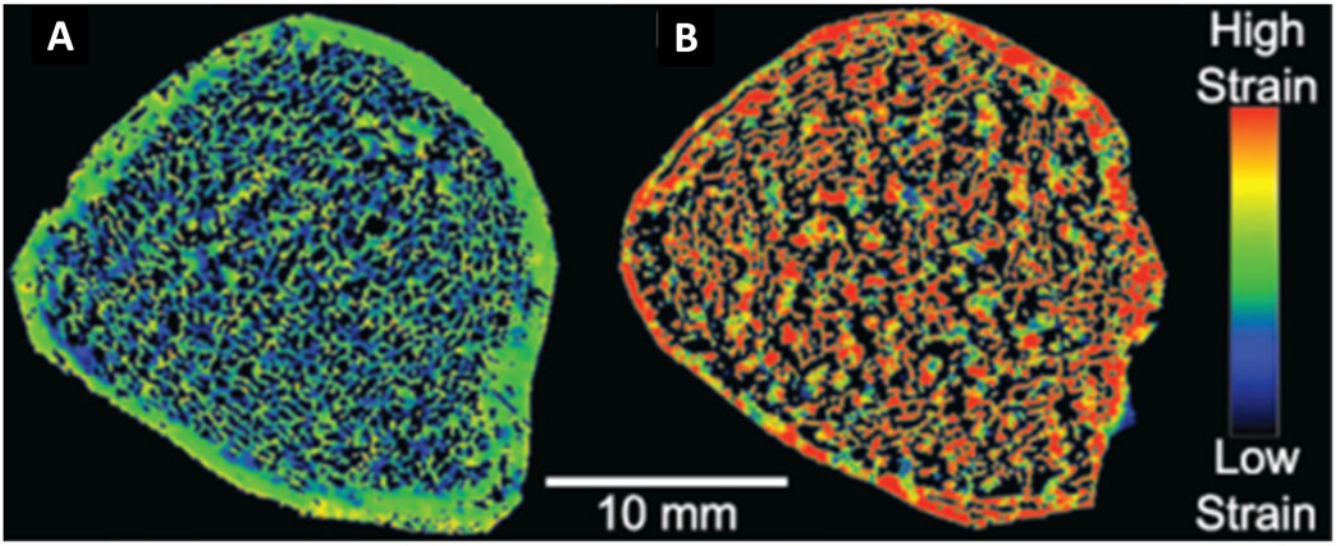

Figure 2:
FE-based strain maps for (A) a representative distal tibial specimen with high mechanical stiffness and strength (thicker cortical bone and well-connected trabeculae) and (B) a representative distal tibial specimen with low mechanical stiffness and strength for a constant mechanical loading. This figure was previously presented by Rajapakse et al. [30]. Reprinting permission is granted through Rightslink. Minor modifications were performed for presentation purposes.

Author Manuscript Author Manuscript Author Manuscript Author Manuscript

Table 1.

Summarized MRI-based micro finite element studies

First author, year	MRI sequence and acquisition	Goal	Finite element (FE) model	Ex/In vivo, Bone site	Results
Van Rietbergen et al. 1998 [40]	• Fast gradient recalled echo (GRE), 1.5T • FOV = 6 cm • Voxel size = 117×117×300 μm • Scan time was not mentioned	• To study the feasibility of MRI-based FEA	• Linear elastic and isotropic element material, 8-node brick elements • Element E = 10 GPa, ν = 0.3 • Special-purpose FE-solver	• Ex vivo • Femoral head • Trabecular bone	• Results of MRI-based models were comparable with μCT-based results; however, correction factors were required.
Newitt et al. 2002 [41][42]	• Fast GRE, 1.5T • FOV ≈ 7 cm • Voxel size = 156×156×500 μm • Scan time ≈ 12 min	• To study the feasibility and reproducibility of in vivo MRI-based FEA	• Linear elastic and isotropic element material, 8-node brick elements • Element E = 10 GPa, ν = 0.3 • Special-purpose FE-solver	• In vivo • Distal radius • Trabecular bone	• Lower elastic measures were found in the osteopenic group compared with the normal group.
Van Rietbergen et al. 2002 [43]	• Fast GRE, 1.5T • FOV ≈ 20 cm • Voxel size = 195×195×500 μm • Scan time ≈ 12 min	• To study the impact of idoxifene treatment on bone mechanics	• Linear elastic and isotropic element material, 8-node brick elements • Element E = 10 GPa, ν = 0.3 • Special-purpose FE-solver	• In vivo • Calcaneus • Trabecular bone	• Significant changes were observed in estimated mechanical properties from baseline within groups after one year of treatment.
Alberich-Bayarri et al. 2008 [62]	• Fast GRE, 3T • FOV ≈ 20 cm • Voxel size = 180×180×180 μm, sub-voxelization to 90×90×90 μm • Scan time ≈ 6 min	• To investigate the FEA feasibility in detecting elastic modulus differences in healthy trabecular bone	• Linear elastic and isotropic element material, 8-node brick elements • Element E = 10 GPa, ν = 0.3 • ANSYS software	• In vivo • Distal radius • Trabecular bone	• FE-based elastic modulus was found to be significantly different between male and female subjects.
Rajapakse et al. 2009 [44]	• Spin Echo (SE), 9.4T • FOV ≈ 0.7 cm • Voxel size = 50×50×50 μm • Scan time ≈ 120 min	• To validate the MRI-based FEA generated from high field (9.4T) scanners	• Linear elastic and isotropic element material, 8-node brick elements • Element E = 15 GPa, ν = 0.3 • FE solver developed in-house	• Ex vivo • Proximal tibia, proximal femur, and lumber vertebrae • Trabecular bone	• Significant strong correlations were observed between estimated moduli from μCT- and MR-based FEA.
Rajapakse et al. 2010 [28]	• Fast large angle spin echo pulse sequence (FLASE), 1.5T • FOV ≈ 5 cm • Voxel size = 160×160×160 μm • Scan time ≈ 40 min	• To validate the MRI-based FEA generated from clinical scanners	• Linear elastic and isotropic element material, 8-node brick elements • Element E = 15 × BVF GPa, ν = 0.3 • FE solver developed in-house	• Ex vivo • Distal tibia • Trabecular bone	• Significant strong correlations were observed between estimated moduli from μCT- and MR-based FEA.
Liu et al. 2010 [68]	• FLASE, 1.5T • FOV ≈ 7×6.4	• To validate the MRI-based	• Linear elastic and isotropic element material, 8-node brick elements	• Ex vivo • Proximal	• Significant strong

Author Manuscript Author Manuscript Author Manuscript Author Manuscript

First author, year	MRI sequence and acquisition	Goal	Finite element (FE) model	Ex/In vivo, Bone site	Results
	cm • Voxel size= 160×160×160 μm • Scan time ≈ 16 min	FEA generated from clinical scanners on whole sections of bone	• Element E=15×BVF GPa, ν = 0.3 • FE solver developed in-house	tibia • Trabecular and cortical bone (whole axial bone section)	correlations were observed between estimated moduli from μCT- and MR-based FEA.
Wehrli *et al. 2010* [69]	• FLASE sequence, 1.5T • FOV ≈ 7×5 cm • Voxel size = 137×137×410 μm • Scan time ≈ 16 min	• To investigate the impact of estrogen supplementation on bone mechanical competence in early postmenopausal women	• Linear elastic and isotropic element material, 8-node brick elements • Element E = 15 × BVF GPa, ν = 0.3 • FE solver developed in-house	• In vivo • Distal tibia and radius • Trabecular bone	• FEA revealed significant reduction and increase in mechanical competence of control group and treated group bone, respectively.
Chang *et al. 2012* [70]	• Fast low angle shot (FLASH) sequence, 7T • FOV = 12 cm • Voxel size = 234×234×1000 μm • Scan time ≈ 7 min	• To investigate the feasibility of performing FEA based on 7T MRI in vivo images	• Linear elastic and isotropic element material, 8-node brick elements • Element E = 15 × BVF GPa, ν = 0.3 • FE solver developed in-house	• In vivo • Proximal tibia and distal femur • Trabecular and cortical bone (whole axial bone sections)	• Large contribution of trabecular bone was seen in whole bone stiffness at the distal femur and proximal tibia.
Chang et al. 2013 [71]	• FLASH sequence, 7T • FOV = 12 cm • Voxel size = 234×234×1000 μm • Scan time ≈ 7 min	• To study the improvements in bone mechanical competence in female dancers	• Linear elastic and isotropic element material, 8-node brick elements • Element E = 15 × BVF GPa, ν = 0.3 • FE solver developed in-house	• In vivo • Distal femur • Trabecular and cortical bone (whole axial bone sections)	• They found greater whole and cancellous bone stiffness, but not greater cortical bone stiffness, in the distal femur of female dancers compared to controls.
Chang et al. 2014 [72]	• FLASH sequence, 3T • FOV = 12 cm • Voxel size = 234×234×1500 μm • Scan time ≈ 25 min	• To study the mechanical differences between patients with fragility fractures and control subjects	• Linear elastic and isotropic element material, 8-node brick elements • Element E = 15 × BVF GPa, ν = 0.3 • FE solver developed in-house	• In vivo • Proximal femur • Trabecular bone	• Patients with fragility fractures showed significantly lower stiffness.
Chang et al. 2015 [73]	• FLASH sequence, 3T • FOV = 12 cm • Voxel size = 234×234×1500 μm • Scan time ≈ 15 min	• To study the reproducibility of linear MRI-based FEA on proximal femur	• Linear elastic and isotropic element material, 8-node brick elements • Element E = 15 × BVF GPa, ν = 0.3 • FE solver developed in-house	• In vivo • Proximal femur • Trabecular bone	• The measurement reproducibility of MR assessment of proximal femur strength is suitable for clinical studies of disease progression or treatment response.
Rajapakse et al. 2012 [63]	• FLASE sequence, 1.5T • FOV ≈ 7×6	• To investigate changes of FEA-based	• Linear elastic and isotropic element material, 8-node brick elements	• In vivo • Distal tibia	• Significant changes in mechanical

Author Manuscript Author Manuscript Author Manuscript Author Manuscript

First author, year	MRI sequence and acquisition	Goal	Finite element (FE) model	Ex/In vivo, Bone site	Results
	cm • Voxel size = 137×137×410 μm • Scan time ≈ 15 min	mechanical properties after renal transplantation	• Element E = 15 × BVF GPa, ν = 0.3 • FE solver developed in-house	• Trabecular and cortical bone (whole axial bone sections)	competence were found after renal transplantation, whereas bone microstructural changes were not significant.
Zhang et al. 2013 [26]	• FLASE sequence, 1.5T • FOV ≈ 7×4 cm • Voxel size = 137×137×410 μm • Scan time ≈ 15 min	• To investigate the feasibility of nonlinear FEA on in vivo data	• Nonlinear Elastic-plastic and isotropic element material, 8-node brick elements • Element E = $\left(\left(\text{sech}(50\times\varepsilon+0.53)^{1.4}\right)^{0.6}+0.05\right)\times BVF\times 15GPa$, ν = 0.3 • FE solver developed in-house	• In vivo • Distal tibia • Trabecular bone	• Potential for providing additional information beyond that obtainable from linear analysis was shown.
Zhang et al. 2013 [27]	• FLASE sequence, 1.5T • FOV ≈ 7×4 cm • Voxel size = 137×137×410 μm • Scan time ≈ 10 min	• To investigate the feasibility of nonlinear FEA on in vivo data for longitudinal studies	• Nonlinear elastic-plastic and isotropic element material, 8-node brick elements • Element E = $\left(\left(\text{sech}(50\times\varepsilon+0.53)^{1.4}\right)^{0.6}+0.05\right)\times BVF\times 15GPa$, ν = 0.3 • FE solver developed in-house	• In vivo • Distal radius • Trabecular bone	• Reproducibility level of the FEA results was adequate for potential follow-up studies.
Rajapakse et al. 2017 [31]	• FLASH sequence, 3T • FOV = 12 cm • Voxel size = 234×234×1500 μm • Scan time ≈ 15 min	• To study the reproducibility of nonlinear MRI-based FEA on proximal femur	• Linear elastic and nonlinear elastic-plastic isotropic element material, 8-node brick elements • Element E = 15 × BVF GP vs. E = $\left(\left(\text{sech}(50\times\varepsilon+0.53)^{1.4}\right)^{0.6}+0.05\right)\times BVF\times 15GPa$, ν = 0.3 • FE solver developed in-house	• In vivo • Proximal femur • Trabecular bone	• The FEA model was able to consistently and reliably provide fracture risk information.
Rajapakse et al. 2018 [30]	• FLASE sequence, 1.5T • FOV ≈ 7×5 cm • Voxel size = 137×137×410 μm • Scan time ≈ 7 min	• To validate linear and nonlinear MRI-based FEA by comparisons with mechanical compression tests	• Linear elastic and nonlinear elastic-plastic isotropic element material, 8-node brick elements • Element E= 15 × BVF GPa vs. E = $\left(\left(\text{sech}(50\times\varepsilon+0.53)^{1.4}\right)^{0.6}+0.05\right)\times BVF\times 15GPa$, ν = 0.3 • FE solver developed in-house	• Ex vivo • Distal tibia • Trabecular and cortical bone (whole axial bone sections)	• Moderate to strong positive correlations were found between computationally and experimentally derived values of stiffness, yield strength, ultimate strength, and resilience.